DOI 10.1007/s10946-024-10193-7
Journal of Russian Laser Research, Volume 45, Number 1, January, 2024

NUMERICAL SIMULATION AND EXPERIMENTAL STUDY OF NANOSECOND PULSED LASER CLEANING OF ALUMINUM ALLOY SURFACE PAINT LAYER

Tanghao Wang, Shanman Lu, Hanqi Liu, Jun Ying, and Wei Zhang*

Jilin Key Laboratory of Solid-State Laser Technology and Application
School of Science, Changchun University of Science and Technology
Changchun 130022, P.R. China

*Corresponding author e-mail: a5371863@163.com

Abstract

In this paper, we present a finite element model that utilizes simulation software to simulate the process of moving nanosecond pulsed laser cleaning on the surface paint layer of 2A12 Aluminum alloy. The objective is to analyze the impact of different laser parameters on the distribution of temperature field within both the paint layer and the substrate surface. Furthermore, we perform experimental validation to verify the findings. The results assume that both laser power and scanning speed influence the outcomes of the cleaning process. At a constant scanning speed, the maximum temperature of both the paint surface and the substrate surface linearly increases with rising laser power. In contrast, at a fixed laser power, the scanning speed influences cleaning outcomes through spot overlap, and the surface temperature of the paint layer rises as the scanning speed decreases. The optimum cleaning effect, with a surface roughness (Ra) of 1.0139 μm, is achieved at a scanning speed of 2500 mm/s and a laser power of 30 W. The surface roughness exhibits first a decrease and then increase pattern with rising laser power. These findings offer valuable insights into process parameters for nanosecond pulsed laser cleaning of surface paint layers on Aluminum alloy.

Keywords: nanosecond pulsed laser, 2A12 Aluminum alloy, finite element model, surface roughness.

1. Introduction

Aluminum alloys are becoming more prevalent in contemporary industries. Due to their light weight, high strength, good plasticity, and corrosion resistance, Aluminum alloys find extensive applications in aerospace, automotive, construction, and various other fields [1,2]. In industrial settings, Aluminum alloy surfaces are frequently painted to enhance corrosion resistance and aesthetics. To ensure the prolonged service life of Aluminum alloys, it is essential to periodically remove and reapply the surface paint layer [3]. Nevertheless, once paint is sprayed onto the surface of an Aluminum alloy, a robust adhesive bond forms between the paint layer and the substrate, rendering the removal of the paint layer challenging. Consequently, finding an efficient and non-destructive method to clean the paint layer sprayed on the surface of Aluminum alloy has emerged as a problem requiring resolution [4]. Common paint removal methods encompass mechanical sanding, chemical treatment, and sandblasting [5]. Nevertheless, these methods pose issues as they are not only time-consuming and inefficient but also result in varying degrees of damage to the Aluminum alloy substrate, impacting its overall service life. Chemical treatments may contribute to environmental pollution and pose potential hazards to human health, among other

Manuscript submitted by the authors in English on December 21, 2023.

1071-2836/24/4501-0106

concerns [6]. Laser cleaning technology represents an efficient, nondestructive, and environmentally friendly approach to surface treatment. Laser cleaning technology employs high-power and high-energy-density laser beams to irradiate the surface paint layer of Aluminum alloy. This process instantly breaks or vaporizes pollutants and surface attachments, achieving effective cleaning of the Aluminum alloy surface paint layer. Laser cleaning offers the benefits of being environmentally friendly, precise, controllable, and highly efficient in comparison to traditional cleaning methods. As a result, it has found extensive application in the industrial sector [7, 8].

In recent years, numerous scholars have conducted research on laser paint removal. Shan et al. [9] explored the effect of laser energy density on cleaning coatings and concluded that the energy density threshold for cleaning paint coatings is 17.69 J/cm^2, the substrate-damage energy-density threshold is 24.77 J/cm^2, and that the cleanliness and integrity of the substrate surface after laser cleaning is the best, when the energy density is 21.33 J/cm^2. Qiu Taiwen et al. [10] carried out laser cleaning of epoxy primer coating on the surface of 2024 Aluminum alloy by changing the laser parameters of pulse frequency and pulse width, discussed the cleaning effect and damage under different laser parameters, and improved and perfected the laser paint removal process. Guo Zhaoheng [11, 12] established a model of nanosecond pulsed laser paint removal and simulated the temperature field distribution of the paint layer under the action of a Gaussian heat source, and found that compared with a spot diameter of 50 μm, a spot diameter of 100 μm can still reach the vaporization temperature of the paint layer, but the peak temperature is lower than the former. Liu Caifei et al. [13] established a finite element model of pulsed laser paint removal, simulated the variation of the temperature field of the paint layer with the laser parameters at different moments, and did relevant comparative experiments. Marimuthu et al. [14] modeled the optimum number of pulses and power to remove contaminants, using a two-dimensional transient method, and described the mechanism of excimer laser cleaning. Mateo et al. [15] found that the lacquer layer on the brass surface could be effectively removed by setting a reasonable laser energy density and repetition frequency. Schweizer et al. [16] found that the laser power density is an important co-variate for paint removal by CO_2 lasers, while the spot overlap rate also has an effect on the paint removal efficiency. Luo Hongxin et al. [17] used a high-power continuous CO_2 laser to clean the paint layer on the surface of the aircraft skin, analyzed the cleaning results, and concluded that the laser paint removal was not a separate mechanism at work, and that its main mechanism was related to the material and physicochemical properties of the paint layer and the substrate, and other factors. Lim et al. [18] performed a finite element simulation of a single nanosecond pulsed laser ablation process based on the thermal evaporation mechanism and verified the effect of parameter variations on the ablation process after comparing it with experimental results.

The previous studies solely simulated the static temperature field distribution of contaminants removed by a single-pulse or continuous laser. However, they did not explore the dynamic temperature distribution resulting from the interaction between a moving pulsed laser and the material. The cleaning process of a moving pulsed laser is achieved through the superposition and overlap of light spots. Consequently, both the scanning speed and laser power density play a crucial role in determining the cleaning effect. To investigate the impact of temperature changes on the cleaning process, in this study, we employ 2A12 Aluminum alloy and epoxy resin primer as materials. We use the finite element simulation software to model the moving nanosecond pulsed laser irradiation on the paint layer surface, with variations in scanning speed and laser power to observe their effects on the temperature field. Subsequently, we conduct nanosecond pulsed laser cleaning experiments to examine the microscopic morphology of the cleaned target material surface, providing insights into the actual cleaning effect. The findings aim to

establish a theoretical and experimental foundation for laser cleaning of the paint layer on the surface of Aluminum alloy.

2. Principles and Theoretical Models

In Fig. 1, we illustrate the principle of laser cleaning. The process of pulsed laser cleaning on the Aluminum alloy surface paint layer can be comprehended as follows: the light source directs laser energy onto the surface of the Aluminum alloy, where the paint layer absorbs the energy, leading to changes in the material temperature. Thermal convection and thermal radiation cause a minor loss of energy, with the majority being instantly absorbed by the paint layer on the Aluminum alloy surface. This rapid absorption attains the gasification temperature of the paint layer, resulting in the effective removal of the paint layer from the Aluminum alloy surface through laser cleaning. Assuming that the laser exclusively interacts with the surface of the paint layer, it is treated as a surface heat source.

Given the complexity of the actual physical process and the numerous factors influencing laser cleaning, in this study, we introduce assumptions to simplify the model during the simulation of its temperature field:

1. The cleaned material is isotropic and its properties do not change with time.
2. The effect of deformation of the material, as it absorbs heat, is not considered.
3. Full thermal conduction between the substrate material and the paint layer.

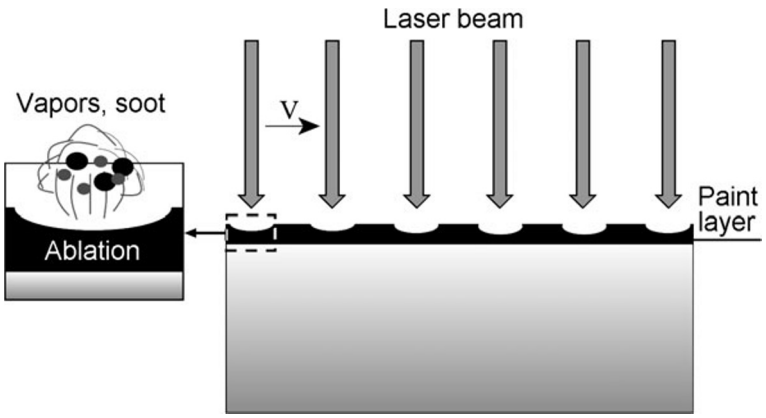

Fig. 1. Principle diagram of laser cleaning.

The model does not consider the impact of gaseous substances, such as plasma generated during the cleaning process, on the absorption of laser energy.

Under the aforementioned assumptions, the differential equations for heat conduction, following the law of energy conservation, read

$$\frac{\partial T}{\partial \tau} = \frac{\lambda}{c\,\rho}\left(\frac{\partial^2 T}{\partial x^2} + \frac{\partial^2 T}{\partial y^2} + \frac{\partial^2 T}{\partial z^2}\right) + \frac{q_m}{c\,\rho}\,. \tag{1}$$

Disregarding the internal heat source of the material, Eq. (1) can be simplified as follows:

$$\frac{\partial T}{\partial \tau} = \frac{\lambda}{c\,\rho}\left(\frac{\partial^2 T}{\partial x^2} + \frac{\partial^2 T}{\partial y^2} + \frac{\partial^2 T}{\partial z^2}\right). \tag{2}$$

In Eqs. (1) and (2), q_m is the energy transferred per unit volume per unit time, τ is the pulse width, c is the heat capacity of the material, λ is the thermal conductivity of the material, and ρ is the density of the material.

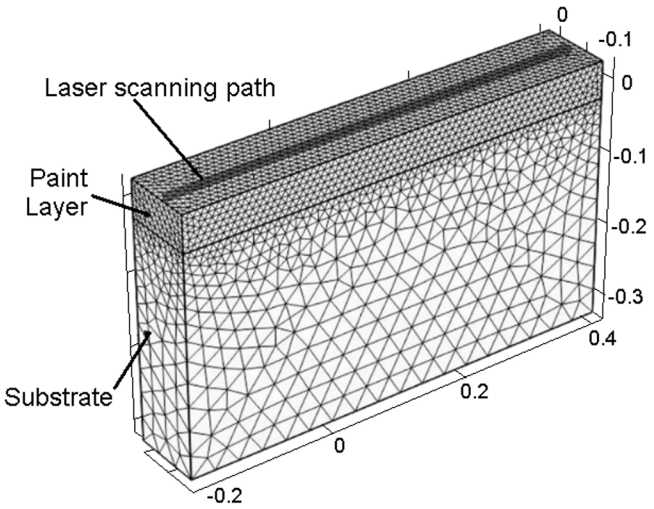

Fig. 2. Finite element model and meshing of the laser-cleaned sample.

In practical terms, given a very small spot radius and a significantly smaller spot area compared to the Aluminum alloy plate, the process can be approximated as a point heat source acting on a semi-infinite object. The simulated temperature changes are [19–21]

$$\Delta T = \frac{Q\sqrt{\alpha\tau}}{0.885\lambda}, \tag{3}$$

$$\alpha = \frac{\lambda}{c\,\rho}\,, \tag{4}$$

$$Q = \frac{P}{\pi R^2}\,, \tag{5}$$

where ΔT represents the temperature change, α is the thermal conductivity of the material, P denotes the laser power, and Q is the power density.

The temperature of the material rises after absorbing the laser energy, and due to the different absorption rates of the laser between the contaminant and the substrate, a thermal expansion effect occurs between the two, and the thermal expansion causes stresses and strains in the material, the thermal expansion length in the z direction can be expressed as follows [22]:

$$\Delta l = l\gamma\Delta T, \tag{6}$$

where γ is the linear coefficient of thermal expansion, ΔT is the temperature difference, and the thermal stresses per unit area of the paint layer-substrate contact surface at $z = l$ are represented by σ_m and σ_n [23], namely,

$$\sigma_m = Y_m\varepsilon_m = Y_m\frac{\Delta l_m}{l_m} = Y_m\gamma_m\Delta T_m(l,t), \tag{7}$$

$$\sigma_n = Y_n\varepsilon_n = Y_n\frac{\Delta l_n}{l_n} = Y_n\gamma_n\Delta T_n(l,t). \tag{8}$$

Here, Y represents the modulus of elasticity, and the adhesion between the paint layer and the substrate can be simplified to the adhesion of two parallel contact surfaces, expressed as follows [24]:

$$f = \frac{A+12}{6z_1^3}\,, \tag{9}$$

with A_{12} being the Hamaker coefficient at the interface and z_1, the distance between the two parallel contact surfaces.

3. Simulation Results and Analysis

3.1. Modeling of Material Geometry

The finite element model is constructed and meshed according to the depiction in Fig. 2. The model dimensions are 0.6×0.1×0.35 mm, featuring two levels – an epoxy primer atop with a thickness of 50 μm,

and a lower layer comprising the 2A12 Aluminum alloy substrate with a thickness of 0.3 mm. The laser scans along the positive x axis of the model. Given that the cleaning process primarily targets the paint layer, finer meshing is applied to the paint layers for enhanced simulation accuracy, whereas coarser meshing is chosen for the Aluminum alloy substrates to reduce computational workload and save time.

Following a review of pertinent information, the thermophysical parameters for the epoxy resin primer and 2A12 Aluminum alloy base material in the simulation are presented in Table 1.

Table 1. Thermophysical Parameters of Epoxy Primers and Aluminum Alloys.

Parameter	Paint	Aluminum alloy
Density, $\mathrm{kg \cdot m^{-3}}$	1300	2800
Thermal Conductivity, $\mathrm{W \cdot m^{-1} \cdot K^{-1}}$	0.3	213
Specific Heat, $\mathrm{J \cdot kg^{-1} \cdot K^{-1}}$	2510	921
Poisson's Ratio	0.2	0.33
Young's Modulus, Pa	$1 \cdot 10^{10}$	$6.9 \cdot 10^{10}$
Thermal Expansion, $\mathrm{K^{-1}}$	$6 \cdot 10^{-6}$	$2.3 \cdot 10^{-5}$
Absorption Coefficient, $\mathrm{cm^{-1}}$	0.6	
Melting Point, K	400 – 410	750 – 820
Boiling Point, K	420 – 430	

3.2. Simulation and Analysis of Its Results

The laser is directed perpendicularly onto the surface of the paint layer, moving swiftly along the positive x axis. Laser powers of 20, 25, 30, 35, and 40 W are individually set, with a spot radius of 25 μm, a laser repetition frequency of 100 kHz, a pulse width of 200 ns, and a scanning speed of 2500 mm/s. This configuration follows the laser power density formula; it reads

$$E = \frac{P}{\pi R^2}\,. \tag{10}$$

Calculation shows that the power density is $1.02 \cdot 10^6$, $1.27 \cdot 10^6$, $1.53 \cdot 10^6$, $1.78 \cdot 10^6$, and $2.04 \cdot 10^6$ $\mathrm{W/cm^2}$, respectively, with P being the average laser power and R, the radius of the spot. Under certain conditions, examining the impact of laser power density on the temperature field distribution is synonymous with evaluating the impact of laser power on the temperature field distribution.

Meanwhile, in Fig. 3, we illustrate the impact of the previously mentioned diverse laser power densities on the temperature distribution of the paint layer on the surface of 2A12 Aluminum alloy.

In Fig. 3, we see that the pulsed laser moves in the positive direction along the x axis, leaving a distinct trace on the surface of the paint work. The temperature field along the trajectory exhibits a Gaussian distribution, with the highest temperature at the center of the laser spot and the lowest at the edges. With increase in the laser power, the range of Gaussian heat source color distributions in the corresponding paint layer surface temperature cloud maps also expands. Due to the rapid heating and cooling characteristics of pulsed laser-heated materials, residual temperature field in the scanning path has not been cooled by previous pulses, and higher laser power increases the temperature of the uncooled temperature field.

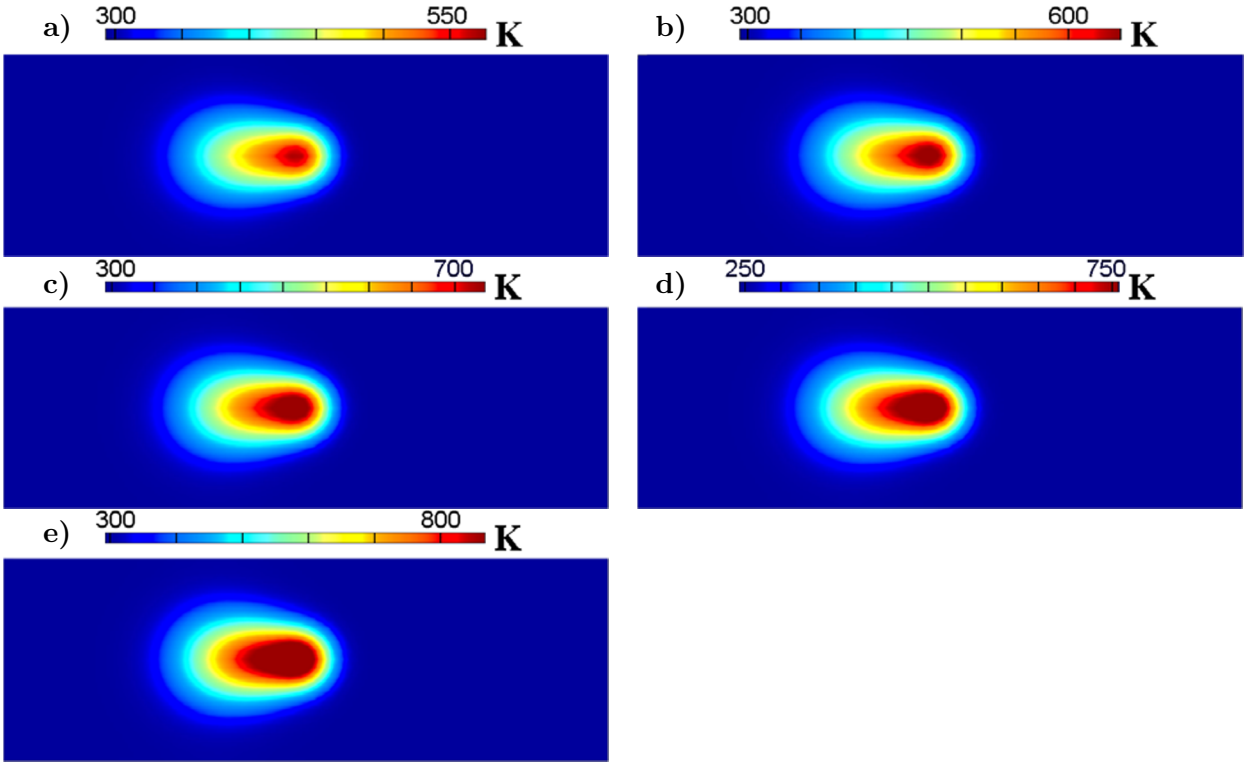

Fig. 3. Temperature distribution of epoxy primer layer at a scanning speed of 2500 mm/s, under different laser power densities equal to $1.02 \cdot 10^6$ W/cm^2 (a), $1.27 \cdot 10^6$ W/cm^2 (b), $1.53 \cdot 10^6$ W/cm^2 (c), $1.78 \cdot 10^6$ W/cm^2 (d), and $2.04 \cdot 10^6$ W/cm^2 (e).

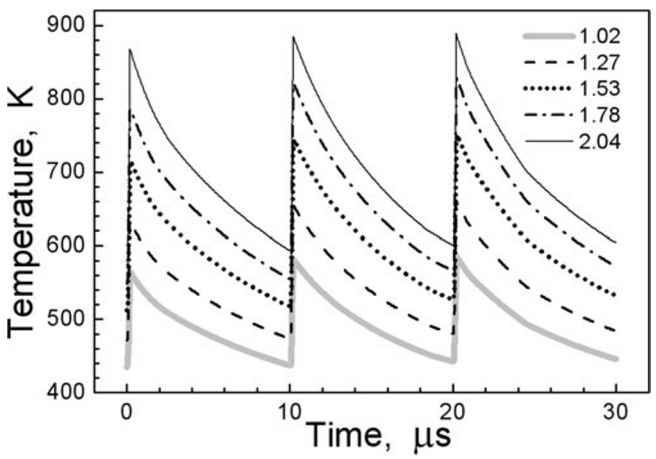

Fig. 4. Variation curve of the paint layer temperature with time at different power densities.

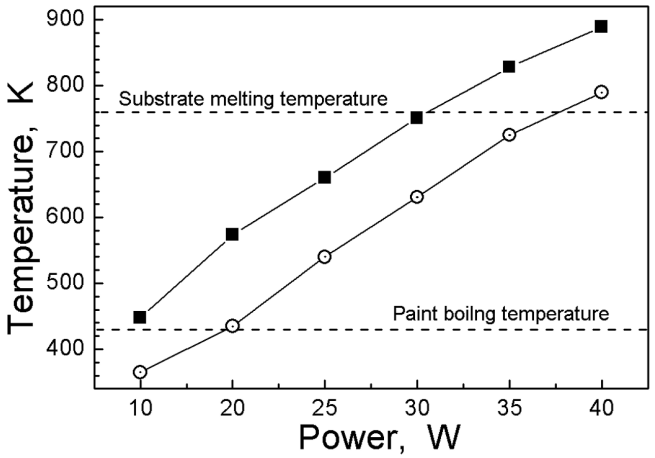

Fig. 5. Maximum temperature curves of the paint surface and substrate surface with different laser powers. Here, paint surface temperature (■) and substrate surface temperature (⊙).

In Fig. 4, with increase in the laser power density, the maximum surface temperature of the paint layer also accordingly rises. Under constant laser power density, the maximum surface temperature of the paint layer rises over time. This results from the heat accumulation effect on the paint layer's surface

when the spot overlap is 50%.

As shown in Fig. 5, with a laser scanning speed of 2500 mm/s and a spot overlap rate of 50%, the temperature changes on the paint layer surface and the Aluminum alloy substrate surface follow a consistent pattern with the laser power. Examining the curve in Fig. 5, when the laser power is 10 W, the maximum temperature of the lacquered surface reaches 448 K, surpassing the gasification temperature of the paint layer. However, the maximum temperature of the substrate surface is 365 K, falling short of the gasification temperature of the paint layer. This indicates that, at this power level, there is residual paint on the substrate surface that has not been cleaned off. At a laser power of 30 W, the maximum temperature of the paint layer surface reaches 751 K, while the Aluminum substrate temperature is 631 K, surpassing the gasification temperature of the paint layer. At this point, the cleaning effect is more pronounced. At a laser power of 40 W, the maximum temperature of the paint surface reaches 889 K. Simultaneously, the maximum temperature of the Aluminum alloy base surface is 790 K, surpassing the melting point of 2A12 Aluminum alloy, resulting in melting on the base surface. With increase in the laser power, more laser energy is absorbed in the laser action area. Specifically, when the spot radius and repetition frequency of the pulsed laser are constant, the laser power increase leads to a proportional rise in the power density. Consequently, the maximum temperature on the surface of the paint layer and the substrate linearly increases.

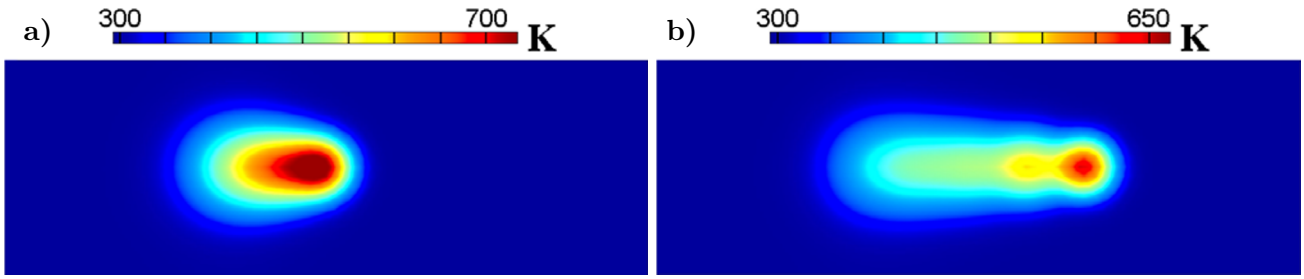

Fig. 6. Distribution of the surface temperature field of the paint layer at two different scanning speeds, namely, scanning speed 2500 mm/s, 50% lap rate (a) and scanning speed 5000 mm/s, 0% lap rate (b). Here, the laser power is 30 W.

In Fig. 6, we illustrate the temperature field distribution of the paint layer for scanning speeds of 2500 and 5000 mm/s, respectively, for illumination with a laser power of 30 W and a repetition frequency of 100 kHz. In Fig. 6 a, we can see that, when the scanning speed is 2500 mm/s and the overlap rate is 50%, each pulse is superimposed by the temperature field to form a bar distribution; because the scanning speed is slower, the heat buildup is relatively high, at this time, and the maximum temperature of the surface of the paint layer is 751.3 K. As shown in Fig. 6 b, the scanning speed is 5000 mm/s, the overlap rate is 0%, and the spot is slightly discrete, the heat build-up effect is almost gone, and the maximum temperature of the paint surface is 667.8 K. Since the spot overlap is 0%, there is no superimposed area between the two pulses, and parts of the paint layer between the spots are not irradiated by the laser energy, resulting in incomplete removal of the paint material.

In Fig. 7, we illustrate the changes in the maximum temperature of the paint surface and the substrate surface with varying laser scanning speeds at a laser power of 30 W, a repetition frequency of 100 kHz, and a spot radius of 25 μm. At a scanning speed of 1000 mm/s, the substrate temperature reaches 765 K, surpassing the melting point of the Aluminum alloy substrate and causing damage. At a scanning speed of 2500 mm/s and a spot overlap rate of 50%, the maximum temperature of the paint layer is 751 K,

surpassing its gasification temperature. When the substrate temperature is 631 K, below the base melting point, the cleaning efficiency is higher.

At a scanning speed of 5000 mm/s and a spot overlap rate of 0%, the surface temperature of the paint layer is 667 K, surpassing its gasification temperature. When the Aluminum alloy substrate temperature is 418 K, below the vaporization temperature of the paint layer, there is some remaining paint layer on the substrate surface. At scanning speeds below 2500 mm/s, with a spot overlap exceeding 50%, the sample temperature rises gradually as the scanning speed decreases. This is attributed to the growing thermal build up resulting from a spot overlap greater than 50%. With a constant repetition frequency and spot radius, higher scanning speeds result in lower spot overlap rates and fewer pulses per unit time. This leads to reduced heat build up, resulting in a relatively lower temperature on the surface of the paint layer.

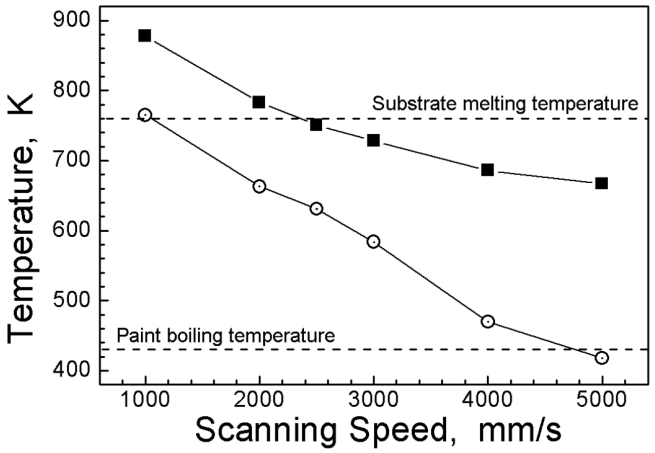

Fig. 7. Maximum temperature curves of the paint surface and substrate surface at different scanning speeds. Here, paint surface temperature (■) and substrate surface temperature (⊙).

4. Pulsed Laser Paint Removal Experiment and Analysis of Results

The 2A12 Aluminum alloy plate utilized in this experiment measures 50×50×2 mm. A modified epoxy resin primer, with a thickness of 50 μm, is applied to its surface. In the experiment, we utilize a nanosecond pulsed laser for cleaning the paint layer on the surface of 2A12 Aluminum alloy. The specific laser parameters are detailed in Table 2. Laser parameters in this experiment include a spot diameter of 50 μm, a repetition frequency of 100 kHz, and laser power ranging from 10 to 40 W. We examine the surface morphology and roughness of the cleaned specimens, using a Leica CTR6000 metallurgical microscope from Leica Microsystems and an Alicona Infinite Focus G5 optical 3D measuring instrument developed by Bruker Alicona in Austria.

Table 2. Parameters of Laser Cleaning Equipment.

Parameter	Value
Wavelength, nm	1064
Laser power, W	≤ 100
Pulse width, ns	100
Focused spot diameter, μm	50
Frequency, kHz	100

Varying the laser power yields the results shown in Fig. 8, depicting the surface micro-morphology and three-dimensional morphology of the Aluminum alloy matrix after cleaning with different power levels. In Fig. 8, at a laser power of 10 W, a significant amount of paint residue remains on the surface of the Aluminum alloy substrate, indicating incomplete cleaning. A more complete layer of paint covering the surface is evident. Overall, there is no discernible change in shape compared to the pre-cleaning state. At a laser power of 20 W, a few micro-pits are visible along the laser path. This occurrence is attributed to the Gaussian distribution of light emitted by the pulsed laser within the focusing range. The center temperature of the Gaussian heat source is capable of reaching the vaporization temperature of the paint layer on the Aluminum alloy substrate surface. However, due to the relatively low power, the paint layer on the substrate surface is not entirely removed, leaving some melted paint residue. Cleaning at this

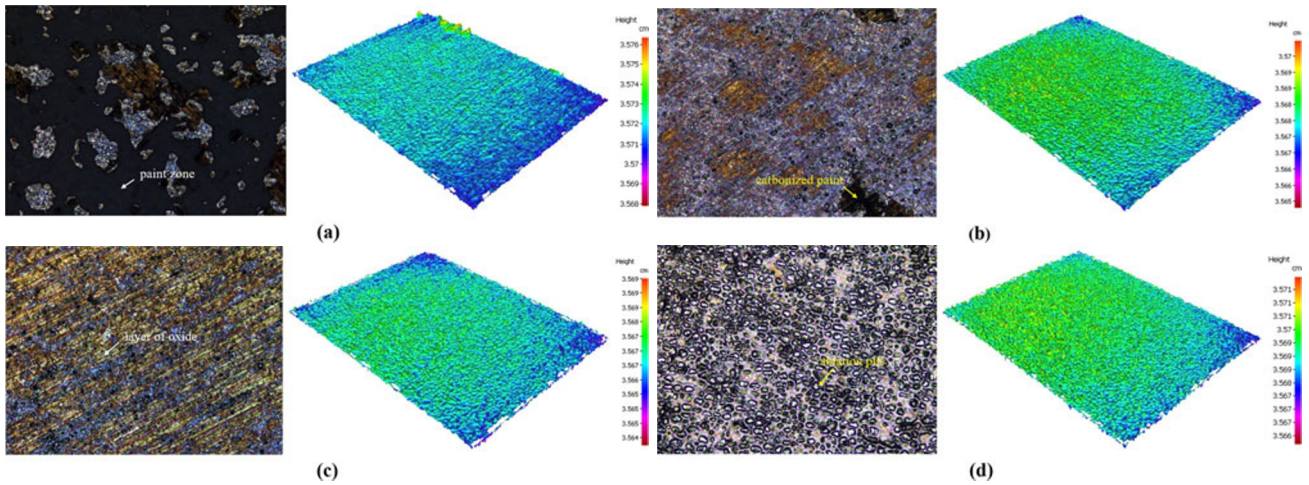

Fig. 8. Morphology and 3D morphology of the substrate surface cleaned by laser with different powers equal to 10 W (a), 20 W (b), 30 W (c), and 40 W (d).

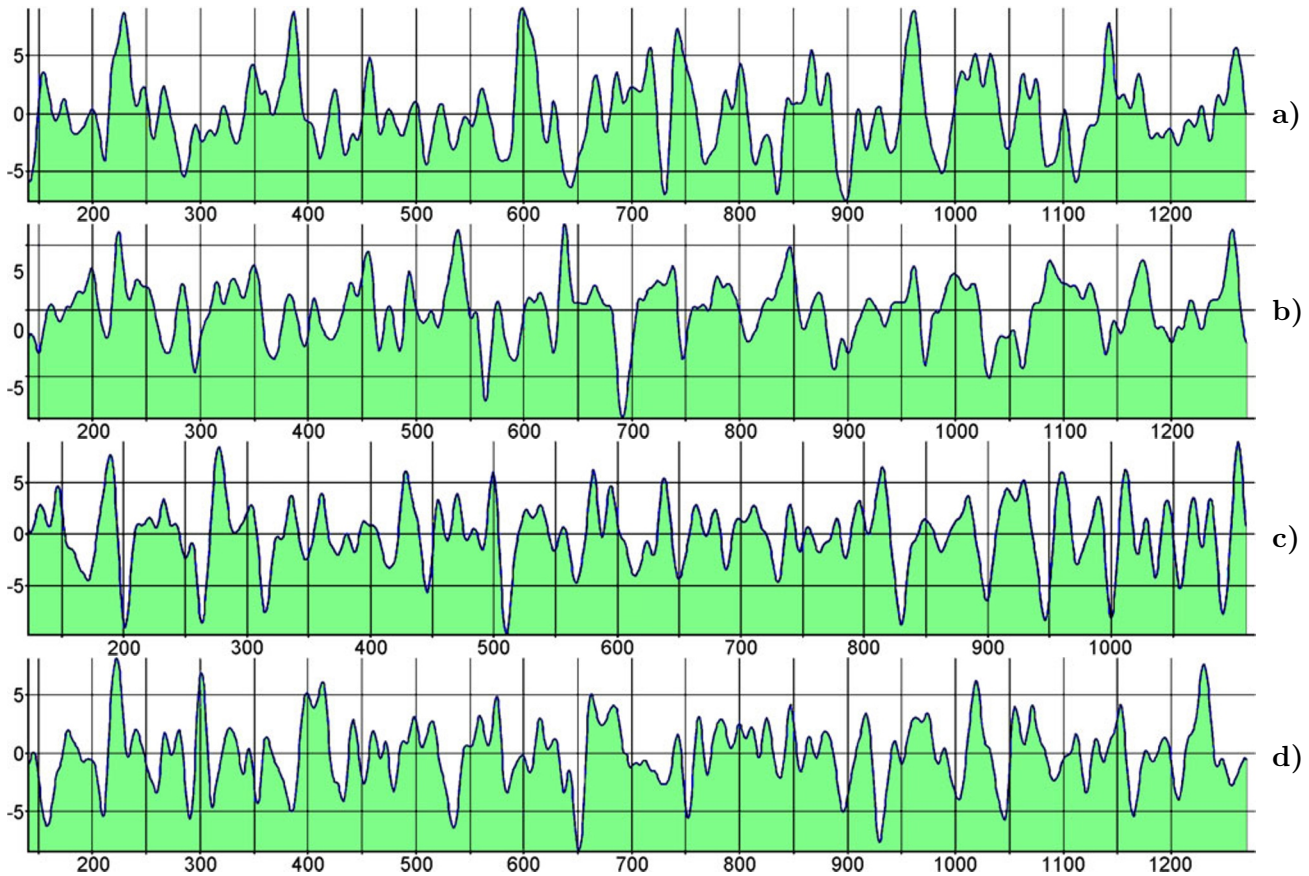

Fig. 9. Surface roughness curves of the samples cleaned with different powers equal to 10 W, with $R_a = 2.58$ μm, $R_q = 3.26$ μm, and $R_z = 14.81$ μm (a), 20 W, with $R_a = 1.84$ μm, $R_q = 2.33$ μm, and $R_z = 11.90$ μm) (b), 30 W, with $R_a = 1.01$ μm, $R_q = 1.31$ μm, and $R_z = 6.15$ μm (c), and 40 W, with $R_a = 2.18$ μm, $R_q = 2.78$ μm, and $R_z = 13.57$ μm (d).

power level is not optimum. At a laser power of 30 W, large areas of yellow oxide film are exposed, and a few ablation pits are formed on the surface of the Aluminum alloy. This is attributed to increase in the power, which elevates the paint material to a temperature suitable for complete vaporization. At this juncture, the cleaning can be considered optimum. At a laser power of 40 W, a significant number of dense pits are observed on the surface of the Aluminum alloy substrate. This results from the ablation of the Aluminum alloy substrate surface and the fusion of the paint layer material, creating uneven pits on the substrate surface. At this power level, the surface of the Aluminum alloy substrate is severely damaged.

The surface roughness of the cleaned Aluminum alloy is assessed using a three-dimensional profilometer. To enhance measurement accuracy, the average value of multiple measurements taken over the same area of the specimen surface is utilized as the surface line roughness (Ra). As shown in Fig. 9, at a laser power of 10 W, only a minimum portion of the laser reaches the surface of the Aluminum alloy substrate. The laser ablates only a small number of micro-pits on the surface of the paint layer, resulting in the highest surface roughness at this power level. At a laser power of 20 W, the laser ablates precisely to the surface of the Aluminum alloy substrate, resulting in small amounts of melted paint and craters on the substrate surface. The surface roughness at this power level is lower compared to 10 W. At a laser power of 30 W, a majority of the lacquer material surpasses the vaporization temperature, with a 50% overlap. Under the effect of temperature superposition, there is uniform ablation of the substrate surface, resulting in smoother marks and minimized roughness. At a laser power of 40 W, the paint layer material significantly surpasses its vaporization temperature. The superposition of temperatures induces melting on the surface of the substrate, leading to substrate surface damage. At this juncture, the roughness is instead elevated.

As observed in Fig. 10, the roughness of the cleaned material surface exhibits a trend of initial decrease and then increase with the increase in the laser power. The optimum cleaning results are attained at a laser power of 30 W, with the surface roughness measuring 1.01 μm.

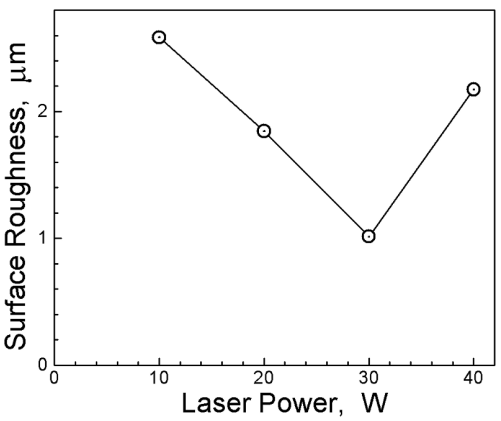

Fig. 10. The curve of the surface roughness of the material with power after cleaning.

5. Conclusions

In summary, in this paper, we modeled the three-dimensional moving nanosecond pulsed laser cleaning of epoxy primer on the surface of 2A12 Aluminum alloy, using simulation and modeling software. We explored the effect of temperature on the surface of the paint layer and the substrate by varying the laser power and scanning speed. The surface of the cleaned material was then experimentally analyzed in a comparative manner. The findings indicate that, when the spot radius and repetition frequency of the pulsed laser are fixed, both laser power and scanning speed influence the cleaning results. At a constant scanning speed, increase in the laser power leads to a linear increase in the maximum temperature of both the paint layer surface and the substrate surface. Specifically, at a laser power of 30 W, the maximum temperature of the substrate surface surpasses the vaporization temperature of the paint layer but does not reach the melting point of the Aluminum alloy base. We obtained the optimum cleaning results under these conditions. At a constant laser power, the scanning speed influenced cleaning results through spot overlap. Specifically, at a scanning speed of

2500 mm/s, with a spot overlap of 50%, the cleaning result was improved, and the cleaning efficiency was higher. With a fixed repetition frequency and spot radius, higher scanning speeds resulted in lower spot overlap rates and fewer pulses per unit time. Consequently, the accumulation of generated heat diminished progressively, leading to a relatively lower temperature on the surface of the paint layer. Through a comparative analysis of the study with the experiments, we concluded that the optimum cleaning results, with a surface roughness (Ra) of 1.0139 μm, were achieved when the spot overlap was 50% and the laser power was set at 30 W. The surface roughness initially decreased and then increased with increase in the laser power.

Acknowledgments

This work was supported by Jilin Provincial Department of Education Fund Project under Grant No. JJKH20230792K.

References

1. F. D. Zhang, H. Liu, C. Suebka, et al.., *Appl. Surf. Sci.*, **435**, 452 (2018).
2. T. Palomar, M. Oujja, I. Llorente, et al., *Appl. Surf. Sci.*, **387**, 118 (2016).
3. A. W. Alshaer, L. Li, and A. Mistry, *Opt. Laser Technol.*, **64**, 162 (2014).
4. Y. M. Chen, L. Z. Zhou, F. Yan, et al., *Chin. J. Lasers*, **44**, 1202005 (2017).
5. G. X. Chen, T. J. Kwee, K. P. Tan, et al., *Appl. Phys. A*, **101**, 249 (2010).
6. S. Siano, J. Agresti, I. Cacciari, et al., *Appl. Phys. A*, **106**, 419 (2012).
7. Y. Kim, J. M. Lee, S. H. Cho, et al., *Opt. Lasers Eng.*, **43**, 1010 (2005).
8. G. X. Chen, T. J. Kwee, K. P. Tan, et al., *Appl. Phys. A*, **101**, 249 (2010).
9. T. Shan, F. Yin, S. Wang, et al., *Appl. Opt.*, **59**, 9313 (2020).
10. T. W. Qiu, J. L. Yi, C. Cheng, et al., *Laser Optoelectron. Prog.*, **58**, 0514001 (2021); DOI: 10.3788/LOP202158.0514001
11. Z. H. Guo, Numerical Simulation and Experimental Research on Nanosecond Pulse Laser Paint Removal, Ph.D. Theses, Jiangsu University, Zhejiang (2020).
12. Z. H. Guo, J. Z. Zhou, X. K. Meng, et al., *China Laser*, **46**, 191 (2019).
13. C. F. Liu, G. Y. Feng, G. L. Deng, et al., *Laser Technol.*, **40**, 274 (2016).
14. S. Marimuthu, A. Mhich, I. S. Molchan, et al., *J. Heat Transfer*, **135**, 121301 (2013).
15. M. P. Mateo, T. Ctvrtnickova, E. Fernandez, et al., *Appl. Surf. Sci.*, **255**, 5579 (2009).
16. G. Schweizer and L. Werner, *Proc. SPIE*, **2502**, 57 (1995).
17. H. X. Lou and Z. G. Cheng, *Laser J.*, **23**, 52 (2002).
18. H. S. Lim and J. Yoo, *J. Mech. Sci. Technol.*, **25**, 1811 (2011).
19. H. C. Zhao, Y. L. Qiao, X. Du, et al., *China Laser*, **48**, 246 (2021).
20. Y. M. Chen, L. Z. Zhou, F. Yan, et al., *Chin. J. Lasers*, **44**, 87 (2017).
21. F. Song, W. F. Zou, B. Tian, et al., *Chin. J. Lasers*, **34**, 1577 (2007).
22. W. F. Zou, Y. M. Xie, X. Xiao, et al., *Chin. Phys. B*, **23**, 433 (2014).
23. Y. Lu, L. Yang, M. Wang, et al., *Appl. Opt.*, **59**, 7652 (2020).
24. A. C. Tam, W. P. Leung, W. Zapka, et al., *J. Appl. Phys.*, **71**, 3515 (1992).